Assessment of the predictive capabilities of discrete element models for flexible rockfall barriers

L. Dugelas, J.B. Coulibaly, Franck Bourrier, Stéphane Lambert, M.A. Chanut, I. Olmedo, François Nicot

Assessment of the predictive capabilities of discrete element models for flexible rockfall barriers

Loïc Dugelas[a,*], Jibril B. Coulibaly[b], Franck Bourrier[c], Stéphane Lambert[c], Marie-Aurélie Chanut[b], Ignacio Olmedo[d], François Nicot[c]

[a] *Univ. Grenoble Alpes, Irstea, LESSEM, 38000 Grenoble, France*
[b] *Geological Hazards Team, Cerema Centre-Est, 25 Avenue François Mitterrand, CS 92803, 69674 Bron Cedex, France*
[c] *Univ. Grenoble Alpes, Irstea, ETNA, 38000 Grenoble, France*
[d] *NGE Fondations, 6 rue de la Métallurgie, 38240 Domène, France*

Abstract

This paper addresses the use of discrete element modeling approaches for predicting the impact response of flexible rockfall protection barriers. In this purpose, two different models are considered and their results are compared to detailed results from full-scale impact experiments. The studied barrier is a prototype made from a 4-contacts ring net and having a 270 kJ nominal capacity. The two discrete elements method models, developed by separate entities with different codes (Yade-DEM and GENEROCK), use different models for the ring net, the cables and cable-net connections, while other structural elements are modelled the same way : posts, anchors, energy dissipating devices, and boulder. The models for the structural elements (ring net, energy dissipating devices) are calibrated individually from quasi-static tensile tests results. The barrier model is then created assembling the structural elements, before being impacted. The tests consist in a impacting in its center a 3-module barrier, first, to one high kinetic energy impact and, second, to three consecutive impacts with a lower kinetic energy. The models results are confronted to measurements made during the experiments, considering a large set of parameters. Both models reveal satisfactory in predicting the structure response, on quantitative and qualitative points of view, and considering the boulder displacement, forces in the main cables and forces acting within the various energy dissipating devices. The quality of the prediction by each model compared to the other depends on the considered parameter. Little deviations from the experimental results are attributed to the model calibration procedure and to slight differences between the real structure and the modeled ones. In the end, the DEM approach appears suitable for modelling flexible barriers in complex loading conditions (high velocity and successive impacts).

Keywords: Rockfall flexible barrier, Experimental, Discrete Element Method, Ring net

*Corresponding author
Email address: loic.dugelas@irstea.fr (Loïc Dugelas)

Introduction

Rockfall is a critical issue in mountainous areas where mitigation measures must be used to protect infrastructures and people from such hazards [Volkwein et al., 2011]. Among the numerous existing protection systems, flexible rockfall barriers are efficient, lightweight and stand as practical solutions to mitigate rockfalls. These barriers are highly deformable structures that can withstand impacts and stop boulders propagating with kinetic energy ranging from 100 kJ up to 10,000 kJ [Lambert and Nicot, 2011]. Determination of rockfall barriers performances has become crucial over time because of their widespread use and the need to guarantee a given protection level. Numerous experimental campaigns have been carried out over the past decades to evaluate the impact energy, i.e. the kinetic energy of the boulder upon impact, one given technology can withstand [McCauley et al., 1985, Smith and Duffy, 1990, Andrew et al., 1998, Muraishi et al., 2005, Peila et al., 1998, Heiss, 2004, Gerber and Böll, 2006, Gottardi and Govoni, 2010, Bertrand et al., 2012]. Insights from experimental campaigns have led to the development of standardized testing methods and guidelines such as the European Assessment Document (EAD) for rockfall protection systems [EOTA, 2018]. Well-instrumented full-scale tests can provide very informative data but require extensive infrastructures and are very costly. In parallel, numerical modeling techniques have been used to simulate impact tests and to obtain new insight into the barrier behavior at a fraction of the full-scale testing costs. Seminal contributions [Nicot et al., 2001b, Cazzani et al., 2002, Volkwein, 2005] introduced new modeling concepts and showed capabilities to simulate the complex nonlinear dynamic response of rockfall barriers under impacts. These works opened the way for the more recent developments taking advantage of increased computational power to implement more complex models [Bertrand et al., 2012, Escallón et al., 2014, 2015, Mentani et al., 2018, Yu et al., 2018], to perform parametric studies [Tran et al., 2013, Spadari et al., 2012, Bourrier et al., 2015, Toe et al., 2018, Castanon-Jano et al., 2018, Coulibaly et al., 2019] and to investigate failure mechanisms [Hambleton et al., 2013, Mentani et al., 2016]. Predictive capabilities of numerical models allow a reduction in the number of full-scale tests to be performed.

The numerical tools used to analyze flexible rockfall barriers present unavoidable limitations, mainly due to the complexity of the dynamic behavior of the structure upon impacts, and the comprehensive assessment of their strengths and limits remains a difficult task. All the modeling codes are readily not available for use, some of them are restrained by intellectual property, and no benchmark or comparative studies between models is known to the authors. Early models have focused on the overall response of the structure. Their coarse discretization and limited complexity do not provide direct access to local information regarding the structure. Recent models have been made increasingly complicated and sometimes unsuitable for current practical engineering applications. To date, there is little quantification of the models capacities to reproduce a given set of properties of a rockfall barrier response. Such quantification should include comparisons of forces, boulder and structure kinematics over the entire loading duration for various loading cases. In the same time, the computational cost of simulations must be kept within reasonable bounds for risk management or industrial time scale of interest. Consequently, the capacities of the model to capture the behavior of rockfall barriers while remaining computationally efficient have to be quantified.

To quantify and compare the capacities of the models, a research group supported by the French national project C2ROP (Rockfall hazards, Protective structures and Risk mitigation) has carried out experimental and numerical research works on a prototype rockfall barrier. C2ROP is an initiative clustering research laboratories, design offices, manufacturers and public authorities around rockfall risk management in mountainous areas. Extensive experimental campaigns were conducted to specify the responses of the components and of the entire barrier under different loading conditions. A deep investigation of the structure response under single and consecutive impacts was made to explore the complex and variable structure response with large deformations and observed asymmetric diffusion of the forces. The experimental data gathered was used to assess the predictive capacities of two models in this complex context. The models, developed independently by contributors of the C2ROP project, are both based on a Discrete Element Method (DEM) but present different modeling features and assumptions.

In the following sections, the prototype barrier is first introduced. Description of the barrier geometry and technology and characterization tests of the barrier individual components as well as full-scale impact tests procedures are detailed in section 1. The two DEM models of the barrier are then detailed and the differences in modeling strategy and assumptions between the two approaches are highlighted in section 2. A detailed description of the response of the barrier based on the experimental full scale tests results is proposed in section 3. This is followed in section 4 by an evaluation of the predictive capacity of both discrete element method models in comparison to the experimental data. A discussion of the strengths, limitations and scope of use of these models is also included in this section.

1. Rockfall barrier

The present section describes the investigated rockfall barrier, in terms of technology, dimensions and position of the elements. The experiments done for the calibration and validation of the structure models are also detailed.

1.1. General description

The prototype rockfall barrier was designed in collaboration between the manufacturers and researchers of the C2ROP Project. The expected capacity of the barrier corresponds to a single centered impact with maximum energy of 270 kJ (corresponding to a boulder with a mass of 740 kg, impacting at a normal velocity of 27 m/s). The barrier is installed on a vertical cliff with a 5° horizontal inclination.

The three modules of the barrier (5 x 2.75 m) are installed between 4 posts, stabilized with 14 cables. A four-contacts ring net (one ring connected to 4 rings - Figure 1) is used. Each net module (11 x 8 rings) is made up of 274 mm diameter rings (mass: 0.25 kg) with a section diameter of 7.5 mm.

The interception net is supported by 10 cables (12 mm diameter) weaved into the external rings (Figure 2.a). The net supporting cables are connected to a post or an anchor by a friction energy dissipating device (Figure 3). All in all, 18 energy dissipating devices connect the cables supporting the net to a post or a lateral anchor. The friction energy dissipating devices work as follow: once the tension in the cable reaches a threshold value, the cable slides in the device and dissipates energy.

Additional upstream, downstream and lateral cables (16 mm diameter) connect the top of the posts to the anchors (Figure 2.b). The posts are the only components subjected to compressive loads. These consist of cylinders, 2.75 m in length and 43.6 kg in mass, with external and internal diameters of 88.9 and 72.9 mm, respectively. The base of the posts is attached to the cliff with an articulated connection leaving the rotation around the longitudinal axis free.

Figure 1: 4-contacts ring net [Coulibaly et al., 2017b].

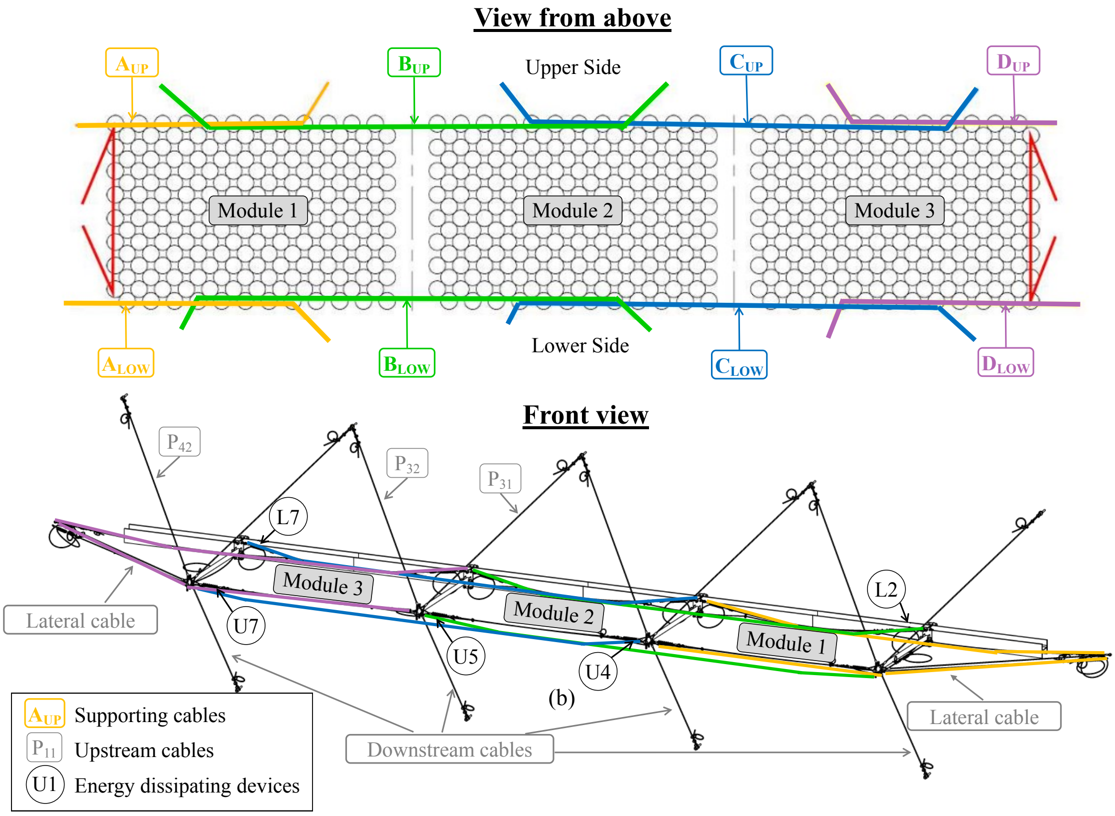

Figure 2: Cables and energy dissipating devices location and identification.

1.2. Elements characterization

For the models calibration (section 2.3), experiments were run to characterize the elements of the barrier. Static loading were chosen because of their set up simplicity, avoiding the launch of a boulder necessary in dynamic experiments. The interception structure and the energy dissipating

Figure 3: Friction energy dissipating device (GTS).

devices were tested into this study, the tests realized are introduced herein. The mechanical specifications of the other elements were taken from literature.

Interception structure

Tensile tests on single rings and on 3 x 3 rings panels were carried out. At the scale of a single ring, two-point (Figure 4.a) and four-point tensile tests (Figure 4.b) were conducted. For the 3 x 3 ring panels, a quasi-static displacement was applied to 3 rings on one side of the panel, while the rings on the opposite side were maintained fixed (Figure 4.c). On the two other sides, translation was possible along the loading direction only. During all these tests, the evolution of the forces at the anchors was recorded against the displacements of these points. A detailed description of these tests can be found in Coulibaly et al. [2017b].

Energy dissipating devices

Three quasi-static tests were conducted with the energy dissipating devices. The devices were installed on a cable fixed at one extremity and subjected to a quasi-static displacement at the other extremity. The force in the cable and the displacement at the moving extremity were both recorded.

1.3. Full scale impact tests

Complete full-scale structures were subjected to both single and consecutive impacts experiments. The impacting boulder was designed following the EAD recommendations [EOTA, 2018]: a polyhedron with an external length of 0.75 m and a mass of 740 kg.

Two tests (SI_{Exp1} and SI_{Exp2}) were performed on two different structures with same characteristics to study the structure response to single centered impacts with energy level at the limit of the structure capacity (270 kJ, with an impact velocity of 27 m/s). The aim was to assess the variability of the experimental results. Second, three consecutive impacts (CO^1_{Exp}, CO^2_{Exp} and CO^3_{Exp}) on the same structure with reduced impact energy (90 kJ, with an impact velocity of 15.6 m/s) were carried out to analyze the structure response when plastic deformations are likely to have developed.

The impacted structures were instrumented with force sensors (acquisition frequency: 10 kHz) to record the evolution of the forces in three upstream cables (P_{31}, P_{32} and P_{42}), and three energy dissipating devices on the supporting cables (L2, L7 and U7) (Figure 2). Two high speed cameras, with a frame rate of 500 Hz, were used to capture the boulder vertical displacement (from the net-boulder contact until the boulder stops) and the global deformation of the structure. A 3600 Hz bandwidth accelerometer was set up in the impacting boulder. After each impact, the elongation of the energy dissipating devices and the elongation of the net were measured. The former will be introduced as the cable elongation, it corresponds to the sum of the maximum elongations of the two energy dissipating devices connected to the studied cable (e.g. the elongation of cable C_{UP} is the sum of the elongations of the devices U4 and U7). For all the measurements, the origin of time (t = 0) corresponds to the instant of contact between the boulder and the net.

Section 3 introduces the results of these full scale tests. The forces recorded with the sensors are explored, as well as the boulder vertical displacement and the elongation of the energy dissipating devices. A deep analysis of the response of the structure under single and consecutive impacts are respectively in section 3.1 and section 3.2.

2. DEM modeling of the barrier

Two models of the barrier presented in section 1 were developed separately. These models are based on the same general principles with different assumptions and modeling strategies.

2.1. General principles

The structure introduced in section 1.1 was modeled using a Discrete Element Method (DEM). This method has been widely used [Nicot et al., 2001a, Bertrand et al., 2008, Thoeni et al., 2013,

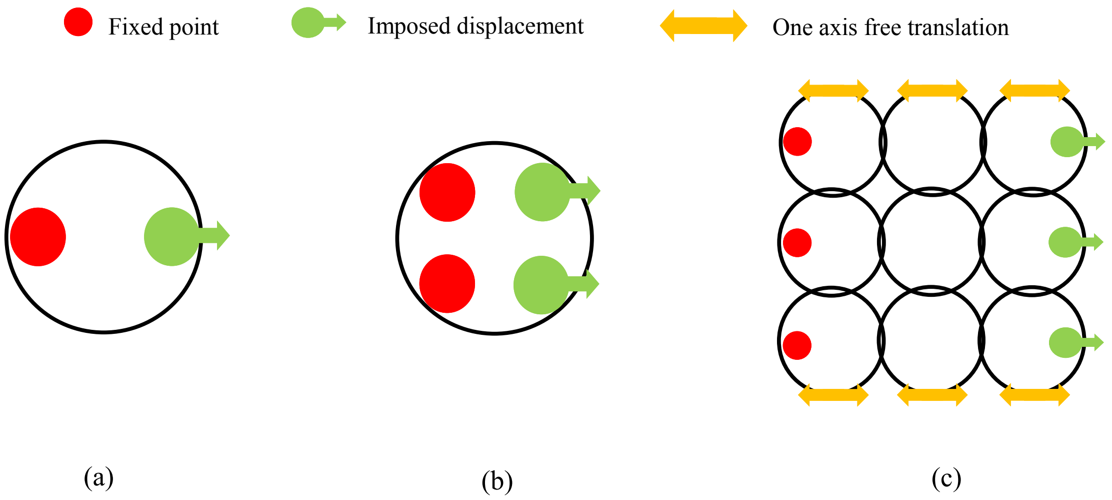

Figure 4: Representation of the tensile tests on the rings: 2 points test (a), 4 points test (b), 3 x 3 rings panel test (c).

Bourrier et al., 2015, Albaba et al., 2017, Coulibaly et al., 2019] to model rockfall protection barriers as it allows explicit and simple integration of large displacements and efficient implementation of multi-body contacts and dynamics. Instead of focusing, as classically in the literature, on a single model of a specific barrier, this study presents two models, developed separately, to analyze the response of the same barrier. The two models (model A and model B) have been developed using the codes Yade-DEM [Šmilauer et al., 2015] and GENEROCK [Coulibaly et al., 2019], respectively. Different assumptions were made, integrating different levels of complexity for the various structure components, besides few elements are modeled in the same way. The different modeling approaches considered are representative of existing ones in the literature. Consequently, the comparison of the models responses gives an overview of the consequences of the modeling choices.

For both models, each element (ring net, cables, energy dissipating devices, posts, connections) is first modeled individually (Section 2.2) and the element models are calibrated (Section 2.3) using data from the static experiments described in section 1.2 and from the literature. Second, the complete barrier is modeled by assembling the element models according to the geometry of the barrier with only rigid assembly between the elements. Finally, the relevance and accuracy of the models are assessed from the analysis of predictive simulations of the impact tests on the full structure described in section 1.3. This assessment is the purpose of section 4.

2.2. Element Models

Retaining net

Two different models of the ring net were used. A 6-contacts ring model developed by Nicot et al. [2001a] (Figure 5.a) was adapted for 4-contacts ring nets and integrated into model A. In this model, each ring is represented by a single spherical particle at its center, and remote interactions model the contacts between neighbouring rings using piece-wise linear force-displacement relationships. These relationships are characterized by three moduli associated with the loading phase and one modulus associated with the unloading one. A more complex ring model [Coulibaly et al., 2017b] was used in model B. This model is based on the location of 4 particles at the contact points between the rings, expect for the external ones (in contact with supporting cables) modeled with three particles. The interactions between these particles are governed by three elasto-plastic constitutive relationships for 2 inner linkages, 4 side linkages and one perimeter linkage (Figure 5.b). The full description of this model is given in Coulibaly et al. [2017b] detailing the 8 parameters for the inner and side linkages (respectively k_d, d_{ih}, a_d, b_d and k_s, s_{ih}, a_s, b_s), and the 6 parameters for the perimeter linkage (k_b, k_t, L_r L_{ih}, a_p, b_p).

Cables

In both models, the cables are modeled by series of articulated elements. These elements are only subjected to tensile forces. Model A describes explicitly the cable as a set of spheres connected by cylinders elements that have the same diameter as the cable. Model B uses material points linked by remote interactions. In both cases, the mass of the cable is distributed to the supporting elements (spheres or material points). 10 and 5 supporting elements per meter are used for model A and model B, respectively.

Cable-net connection

The complex interlacing between the net and the supporting cables plays an important role in the structure response. The so-called curtain effect resulting from this sliding has been shown to have a significant influence on the structure response [Coulibaly et al., 2019]. In the first model, it is accounted for using sliding rings located at the attachment points of the net on the cables (Figure 6), as per Albaba et al. [2017]. The sliding rings, made up of four rigid cylinders, surround the supporting cable and interact with it using an elasto-frictional contact model. In model B, a frictional sliding model of the points of the cables connected to the net is implemented [Coulibaly et al., 2018]. Model B describes this system as a collection of sliding and non-sliding nodes, corresponding to the net and cable respectively. The complete presentation of this model is given in Coulibaly et al. [2018].

Posts

The posts are modeled as cylindrical beams in model A (11 cylinder elements of 0.25 m length for each post) whereas they are assumed to be rigid in model B.

Energy dissipating devices

The same model was used for the energy dissipating devices in both models. It consists in two particles initially spaced by the length of the device and linked by a remote interaction. A 3 parameters (threshold force Fy, elastic modulus K_1 and plastic modulus K_2) elasto-plastic Prager model is used to describe the mechanical behavior of the dissipating devices observed in quasi-static experiments (section 1.2).

Anchors and boulder

The same modeling assumption was taken for anchors and boulder as well. The anchors are modeled as fixed points and the impacting boulder is modeled as a rigid body, with a geometry in accordance with the EAD recommendation [EOTA, 2018]. The boulder interacts with the net using an elasto-frictional contact model.

The modeling assumptions associated with models A and B are summarized in Table 1.

2.3. Models Calibration

All the parameters of the element models introduced in section 2.2 are calibrated using data from the experimental campaign described in section 1.2, or from literature data. This section describes the calibration process for each component and refers to existing documents where more details concerning the calibration can be found. The interception structure and energy dissipating devices are calibrated using specific experimental data, while the other elements are calibrated using literature data.

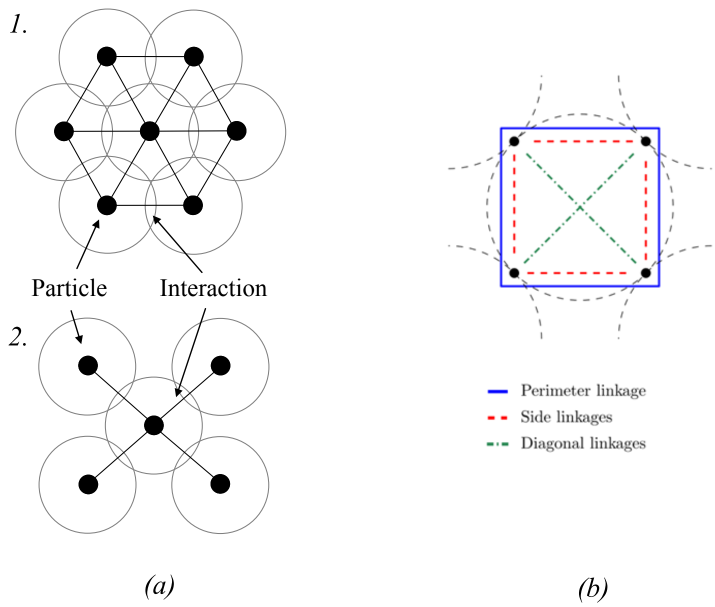

Figure 5: Nicot's 6-contacts ring net model [Nicot et al., 2001a] (a.1), 4-contacts ring net adapted model (a.2), Coulibaly's 4-nodes ring model [Coulibaly et al., 2017b].

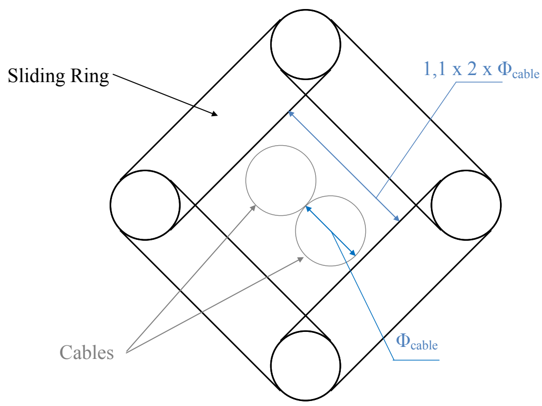

Figure 6: Sliding ring model from Albaba et al. [2017].

Component	model A	model B
Ring Net	Adaptation of Nicot's model [Nicot et al., 2001a]	Coulibaly's ring model [Coulibaly et al., 2017b]
Cables	Succession of articulated rigid plain cylinders 10 nodes per meters	Articulated rigid elements 5 nodes per meters
Energy dissipating devices	Two particles linked by remote interaction	
Posts	Succession of articulated rigid plain cylinders	Rigid rod
Anchors	Fixed points	
Cable-net link	Sliding rings model [Albaba et al., 2017]	Sliding nodes model [Coulibaly et al., 2018]
boulder	Polyhedron shape rigid body	

Table 1: Modeling assumptions for models A and B.

Retaining net

The net model integrated in model A is calibrated using the results of quasi-static tensile tests on 3 x 3 rings panels (Section 1.2). The calibration allows to fit the experimental response using a three-linear curve (Figure 7). The values of calibration parameters are specified in table 2. The 14 parameters of the ring net model used in model B were calibrated using 2 points and 4 points quasi-static tensile tests. The complete detailed calibration process is available in Coulibaly et al. [2017b] (Section “Model Calibration”) and the parameters values from Coulibaly [2017a] (Chapter 5, section 3) are presented in table 3.

Energy dissipating devices

The energy dissipating device model is similar in model A and B. It is calibrated from quasi-static tests. Quasi-static tests are faster and easier to set up than dynamic ones, where the launch of a boulder is needed. They also guarantee more reproducible loading conditions and, thus, exhibit smaller variability. The values for the 3 parameters of the model are $F_y = 25$ kN, $K_1 = 250$ kN/m and $K_2 = 7.143$ kN/m (Figure 8). It must be noted that the response of energy dissipating devices to realistic dynamic loading conditions is expected to be slighly different from quasi-static ones [Castanon-Jano et al., 2017].

Other elements

Finally, the parameters of the cables and posts models are calibrated using information obtained from the literature and from the manufacturers [Feyrer, 2015] detailed in table 4. The cable-net interaction, controlled by frictional processes, is characterized by a friction coefficient of 0.18, as proposed by Albaba et al. [2017] for model A, whereas a friction coefficient of 0.3 is chosen for model B [Coulibaly, 2017a].

Elongation range (m)	Modulus (kN/m)
0 - 0.058	44
0.058 - 0.082	256
0.082 - 0.1	1667
> 0.1	Failure

Table 2: Model A net interaction calibration parameters.

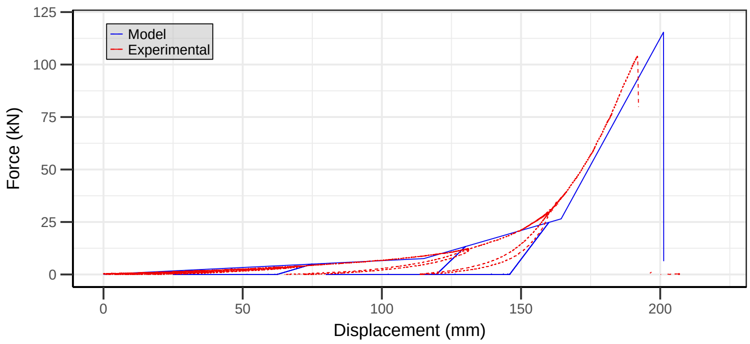

Figure 7: Force over displacement for tensile test on 3 x 3 rings: net model A results against experimental results.

Parameter	Value (3 nodes)	Value (4 nodes)
k_b (N/m)	15533	28106
k_t (N/m)	1450446	1684249
k_d (N/m)	70120	2893
k_s (N/m)	10787	10787
L_r (m)	0.8524	0.8475
L_{ih} (m)	0.700	0.7749
d_{ih} (m)	0.2531	0.314
s_{ih} (m)	0.1938	0.1938
a_p	1731	30479
a_d	0	4955179
a_s	0	0
b_p	3.163	3.588
b_d	0	5.198
b_s	0	0

Table 3: Model B net linkages calibration parameters [Coulibaly, 2017a].

Cable	Upstream	Downstream	Lateral	Supporting
Diameter (mm)	16	16	16	12
Linear mass (kg/m)	0.98	0.98	0.98	0.55
Failure force (kN) (from manufacturer)	168	168	168	94
Young Modulus (GPa)	100	100	100	100

Table 4: Cables properties.

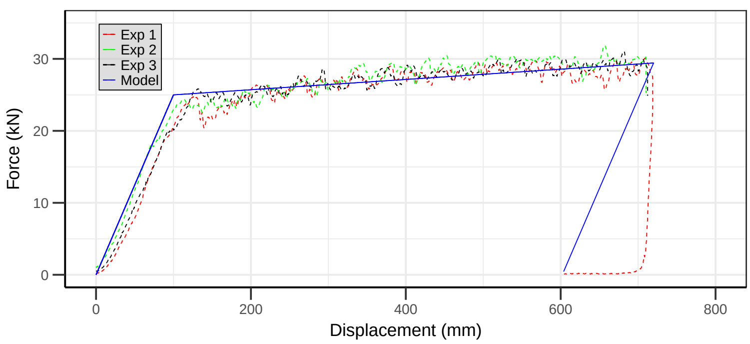

Figure 8: Force over energy dissipating device displacement along quasi-static tensile loading paths: Prager model results against experimental results.

2.4. Simulation campaign

Both a "single impact" simulation and a "consecutive impacts" simulation were performed. The "single impact" simulation consists of one 270 kJ energy centered impact (740 kg boulder with an impact velocity of 27 m/s). The "consecutive impacts" simulation consists of 3 consecutive impacts at a 90 kJ energy level (740 kg boulder, 15.6 m/s), corresponding to one third of the energy level of the "single impact" simulation.

The barrier models are created using the design introduced in section 1.1. On-site geometrical adjustments during the installation of the full scale barrier and small variations in the impact point location were not considered.

Before each impact simulation, the barrier model is left for 2 seconds under gravity loading. For the single impact, the following phase consists of the impact, lasting 0.75 s. For the consecutive impact simulations, a first impact is run during 0.4 sec. When the boulder reaches static equilibrium, it is removed. The barrier is then left under gravity, until it reaches a second equilibrium state without boulder. The second and third impacts are simulated, following the same procedure (Figure 9).

The same timestep, set at $\tau = 10^{-5}$ s, is used for all simulations and for both models. For model A, the "consecutive impacts" simulation (gravity deposition and three impacts - Figure 9) requires 2175 seconds computation time using an Intel Core i7-6820HQ CPU 2.70 GHz CPU, which corresponds to a temporal factor (simulation time/simulated time) of 102.5. For model B, it requires 2671 seconds to simulate the consecutive impacts test using an Intel Core i3-4100M 2.50 GHz CPU, giving a temporal factor of 126. The comparison between the two models, in terms of their ability in predicting the structure response, is thus not biased by any significant difference in computation time efficiency.

For all impact tests, classical quantities used for assessment purposes according to the EAD recommendations [EOTA, 2018] are monitored. The residual height of the barrier after impact, defined as the horizontal distance between the supporting cables after impact. Also, the boulder vertical displacement is recorded from the beginning of the impact (net-boulder contact) until it stops.

Quantities of specific interest for the design of flexible barriers are also measured. The analysis focuses on the evolution of the forces into three energy dissipating devices (L2, L7 and U7 - Figure 2), on the evolution of the forces in three upstream cables (P_{31}, P_{32} and P_{42} - Figure 2), and on the maximum elongation of each energy dissipating devices.

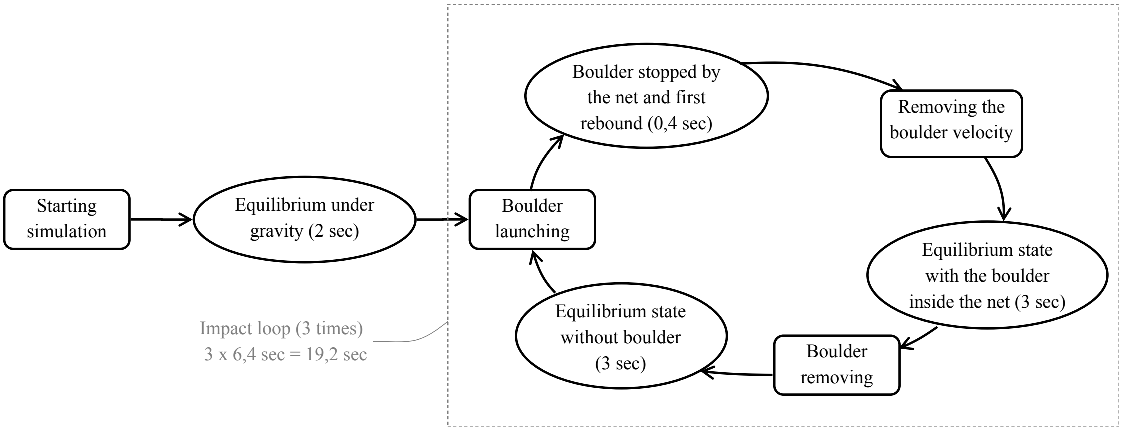

Figure 9: Simulation steps.

3. Structure response

The response of the structure is presented and discussed based on the real-time measurements of the boulder vertical displacement, cable elongation and forces acting on the energy dissipating devices and in the upstream cables. This analysis aims at highlighting trends and specific features of the spatial-temporal response of the structure during the single and the consecutive impacts tests.

3.1. Single impact test

The two single impact experiments (SI_{Exp1} and SI_{Exp2}) show qualitatively similar responses for the barrier in terms of rock block braking (Figure 10), exhibiting two distinct phases, from the very beginning of the boulder-structure contact (t=0).

During the first phase, defined as the pre-tensile phase ($t < 70$ ms, approximately), the boulder velocity exhibits negligible variation as shown by the linear evolution of the vertical displacement over time. No significant resisting force is applied to the boulder during this phase because the net is subjected to geometrical rearrangements (Figure 10). This phase is associated to a change in the net geometrical configuration until high tensile forces develop into the net. These forces are progressively transmitted towards the other structure components, in particular the energy dissipating devices until their activation as observed in figure 11. In the same time, sliding of the net on the supporting cables was observed with the high speed cameras.

The energy dissipating devices activation induces an increase in the length of the supporting cables devices. This modifies the shape of the complete structure favouring a direct transfer of the forces from the impact zone to the anchors, through the energy dissipating devices. This corresponds to the second phase of the structure response (namely the reaction phase) with significant resisting force applied to the boulder, inducing a decrease in its velocity, i.e. a non-linear evolution of its vertical displacement (Figure 10).

The temporal response trend of the energy dissipating devices is similar for all devices and for the two impact tests (Figure 11). The force increases regularly till a threshold value is reached (around 20 kN), which corresponds to the device activation. The force then oscillates around this threshold value.

Similar evolution of the forces in the upstream cables is observed for the two impact tests (Figure 13). During the pre-tensile phase, a higher force is observed in cable P_{32} than in cable P_{31}. At the beginning of the reaction phase, the force in P_{32} starts decreasing till $t = 120$ ms approximately, before increasing again. In contrast, the force in P_{31} regularly increases until $t = 200$ ms. These differences may be explained by the close relationships between the forces in the upstream cables and the motion of the post extremity these cables are connected to. During the pre-tensile phase, the progressive deformation of the net central panel induces a displacement of the extremity of the two central posts towards the center of the barrier. It entails a larger force in P_{32} than in P_{31} (Figure 13). At the beginning of the reaction phase, the activation of the energy dissipating devices U5 and U7 increases the length of the supporting cables B_{UP} and C_{UP}, and the net stops its motion toward the center of the barrier. It moves downward as the boulder continues moving downward, which induces a motion of the posts both downward and towards their initial lateral position. This motion first results in a decrease in the force in P_{32} and in an increase in P_{31} (Figure 11). When the initial lateral position of the posts is reached, the forces increase both in P_{31} and P_{32}. Cable P_{42} experiences a more progressive loading and a lower maximum force than cables P_{31} and P_{32} because it is located further from the impact zone.

Finally, in both tests, the forces in the energy dissipating devices L2 and L7 suggest asymmetrical lateral diffusion of the forces into the barrier (Figure 11). This is confirmed by the different maximum elongations of the cables associated with these energy dissipating devices in figure 12 (SI_{Exp1}: 220 cm for the cable B_{LOW} (L2) and 247 cm for C_{LOW} (L7), SI_{Exp2}: 257 cm and 280 cm for the same quantities).

Despite the similar qualitative responses between the two tests, quantitative differences are evidenced. First, for the first impact, SI_{Exp1}, the boulder is stopped earlier (Figure 10) and the forces in the energy dissipating devices and in the upstream cables also vanish earlier (Figure 11 and 13). One can deduce that the impact duration is shorter in SI_{Exp1} than in SI_{Exp2}. In addition, a shorter penetration is observed for SI_{Exp1}. Second, the response of the energy dissipating devices is highly different from one test to the other and from one device to the other (Figure 11 and 12). Significant differences in the maximum elongations of the cables are also observed, e.g. B_{LOW} : 220 cm for SI_{Exp1} and 257 cm for SI_{Exp2}. Finally, the time evolution of the forces in the upstream cables are quantitatively different, and in particular that of cable P_{32} with different values and times for the maximum forces peaks (24 kN and 26 kN at respectively 90 ms and 250 ms for SI_{Exp1}, and 10 kN and 32 kN at respectively 75 ms and 215 ms for SI_{Exp2}). These results clearly reveal the difference in response from one structure to the other.

These qualitative and quantitative analyses exhibit the structure response complexity, variability and sensitivity for two similar structures subjected to an similar impact. The two tests provide different responses and force distributions inside the structure. An asymmetrical behavior is also observed for the force distribution and energy dissipating devices elongation. These observations are attributed to little differences in the structure installation in terms of initial tension in cables and exact geometry in particular, as well to the energy dissipating devices response variability. Considering these differences highlighted between two similar impacts, we cannot expect one given experimental result to be the representative response of the structure, but we can consider it as one outcome.

3.2. Consecutive impacts test

The structure was subjected to 3 consecutive impacts experiments (CO^1_{Exp}, CO^2_{Exp} and CO^3_{Exp}) at energies three times lower than for the single impact tests (90 kJ energy - corresponding to a 740 kg boulder at a velocity of 15.6 m/s). This test was performed without any repair nor maintenance

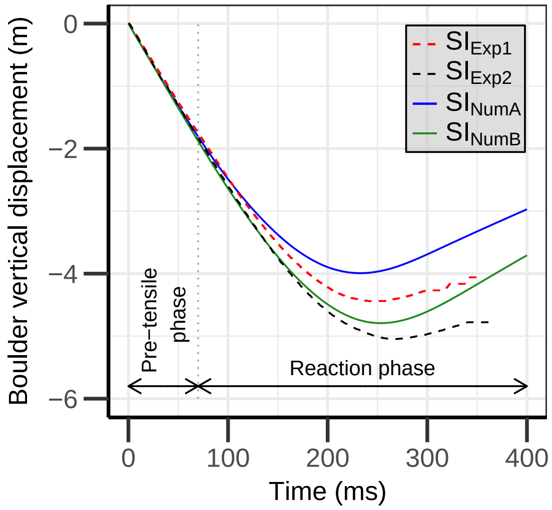

Figure 10: Boulder vertical displacement over time for single impact test: simulation results for models A and B, against the experimental data.

work. Due to recording issues, no real-time data were collected from the sensors during CO^2_{Exp} but the other measurements are available.

As for the single impact tests (section 3.1), pre-tensile and reaction phases are observed in the structure response. They are clearly identified for the first impact CO^1_{Exp} with linear and non-linear parts on the curve giving the boulder vertical displacement over time but are almost absent for the third impact CO^3_{Exp} (figure 14). Qualitative similarities between the single impact tests and the first impact CO^1_{Exp} are also observed for the energy dissipating devices (Figure 15) and the upstream cables responses (Figure 16). During the first impact, the structure reorganizes in a geometrical configuration favoring the energy transfers from the impact zone to the anchors.

In the consecutive impacts, the initial configuration corresponds to the end of the previous impact after bloc removal and smaller geometrical changes are observed. As the duration of the pre-tensile phase is very limited for CO^3_{Exp}, the boulder almost decelerates from the impact beginning. Hence, shorter impact duration and boulder maximum displacement are observed (3.56 m and 1.20 m for respectively impacts 1 and 3) (Figure 14). In addition, the energy dissipating devices are activated earlier and their activation duration is about twice lower for CO^3_{Exp} compared to CO^1_{Exp} (figure 15). The forces in the upstream cables increase faster, from the impact beginning, and reach higher maximum values for the third impact (figure 16). This means that the top of the posts does not initially move towards the center of the barrier. These observations demonstrate

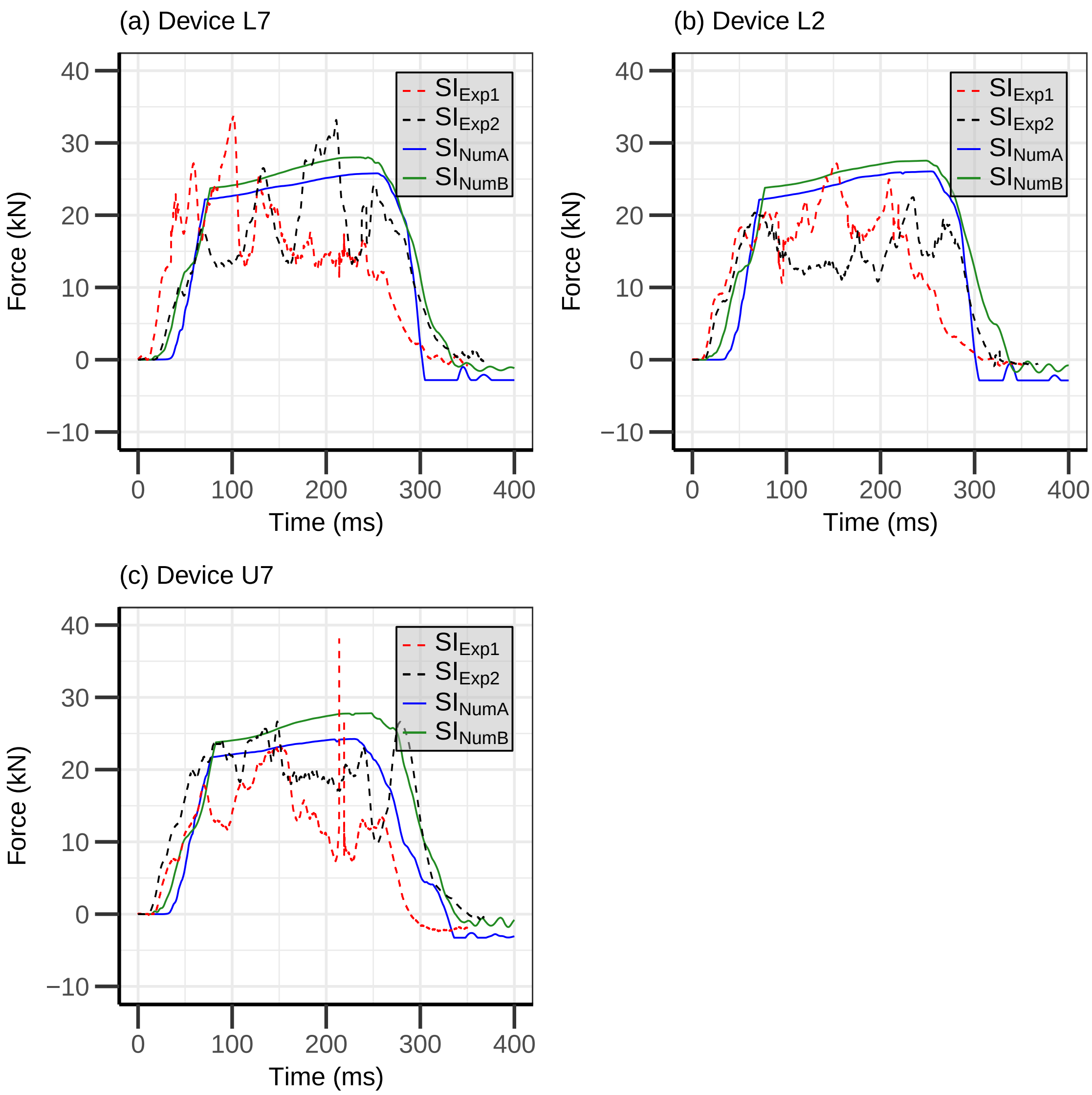

Figure 11: Evolution of the force acting within the energy dissipating devices, simulation results for models A and B against the experimental data: Device L7 (a), Device L2 (b), Device U7 (c).

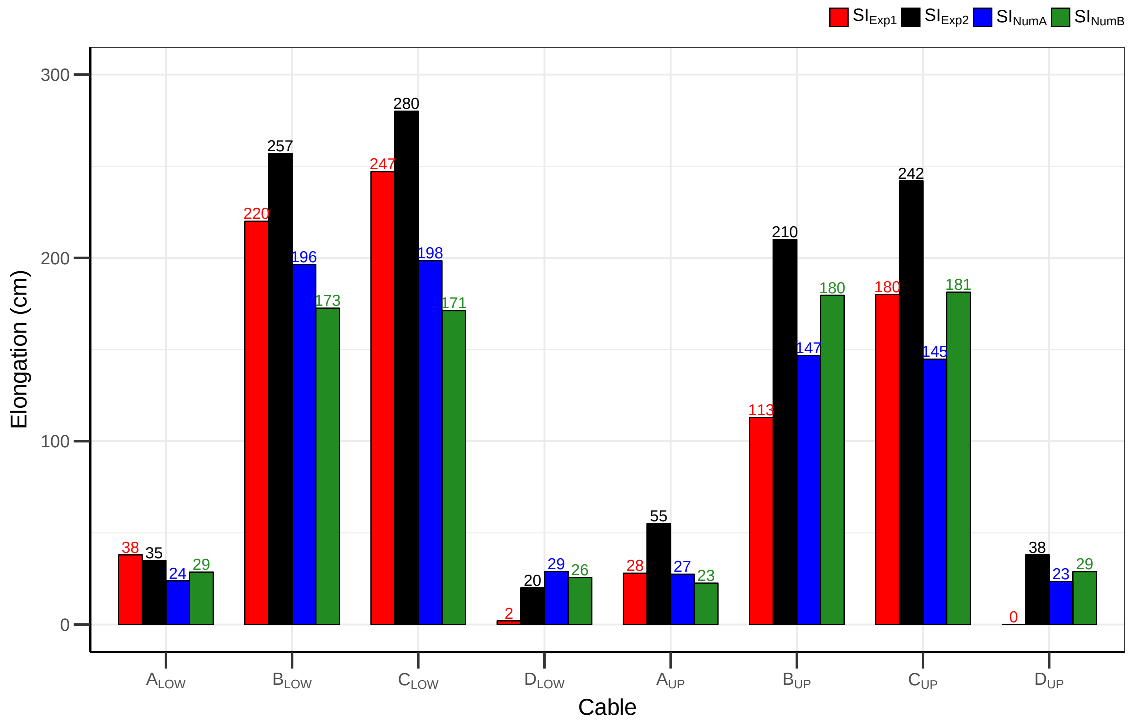

Figure 12: Cables elongation (sum of the elongations of the two energy dissipating devices connected to the cable) after impact for single impact tests, simulation results for models A and B against the experimental data.

an overall stiffer structure response for the third impact.

The post-impact elongation of the cables (table 5) evolves over the consecutive impact as well as it confirms the asymmetrical response of the structure. As for the evolution, results show that the cables elongation is higher during the first impact, when both considering the elongation of single cables and the sum of the elongations of all the cables. As for the asymmetrical response, higher elongations are observed for all three tests on upper cables A and B than in upper cables C and D, located on the other side of the structure with respect to the impact point. The opposite trend is observed focusing on the lower supporting cables, with higher values on cables C and D than in cables A and B. Comparison between upper and lower supporting cables also reveals that, in this latter case, elongations in the central part are lower (cables B and C) than in the former case.

The results from the first of the consecutive impact tests (CO^1_{Exp}) confirm the nature of the mechanical response of the structure to a single impact test. A different response is observed for the third impact (CO^3_{Exp}) with a very limited pre-tensile phase, leading to a stiffening of the structure. Similar as for the single impact tests, an asymmetrical response is observed in terms of

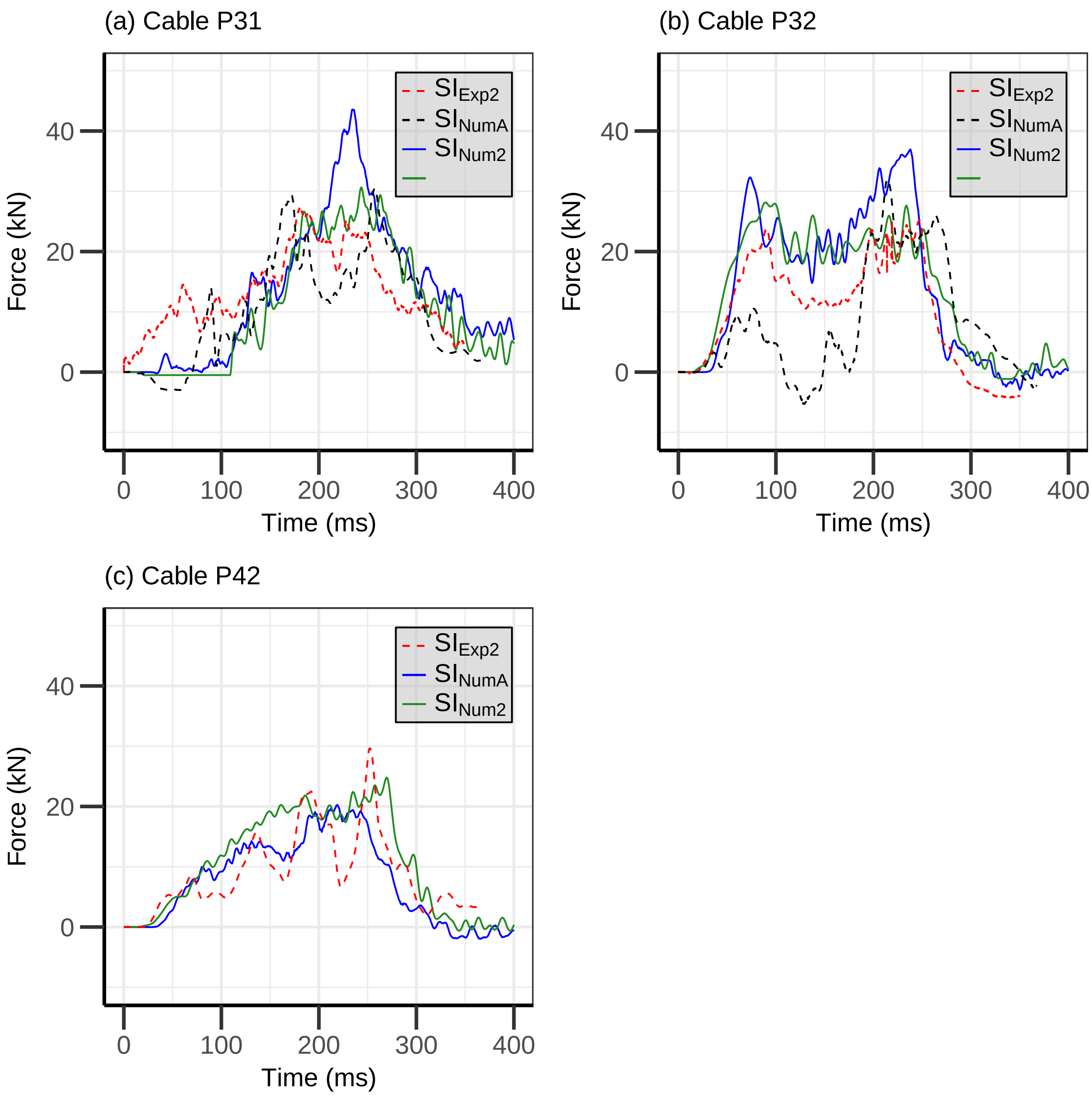

Figure 13: Evolution of the force acting into the upstream cables for single impact test, simulation results for models A and B against the experimental data: Cable P_{31} (a), Cable P_{32} (b), Cable P_{42} (c).

elongations of the energy dissipating devices and forces evolution in the structure components, for all impact tests.

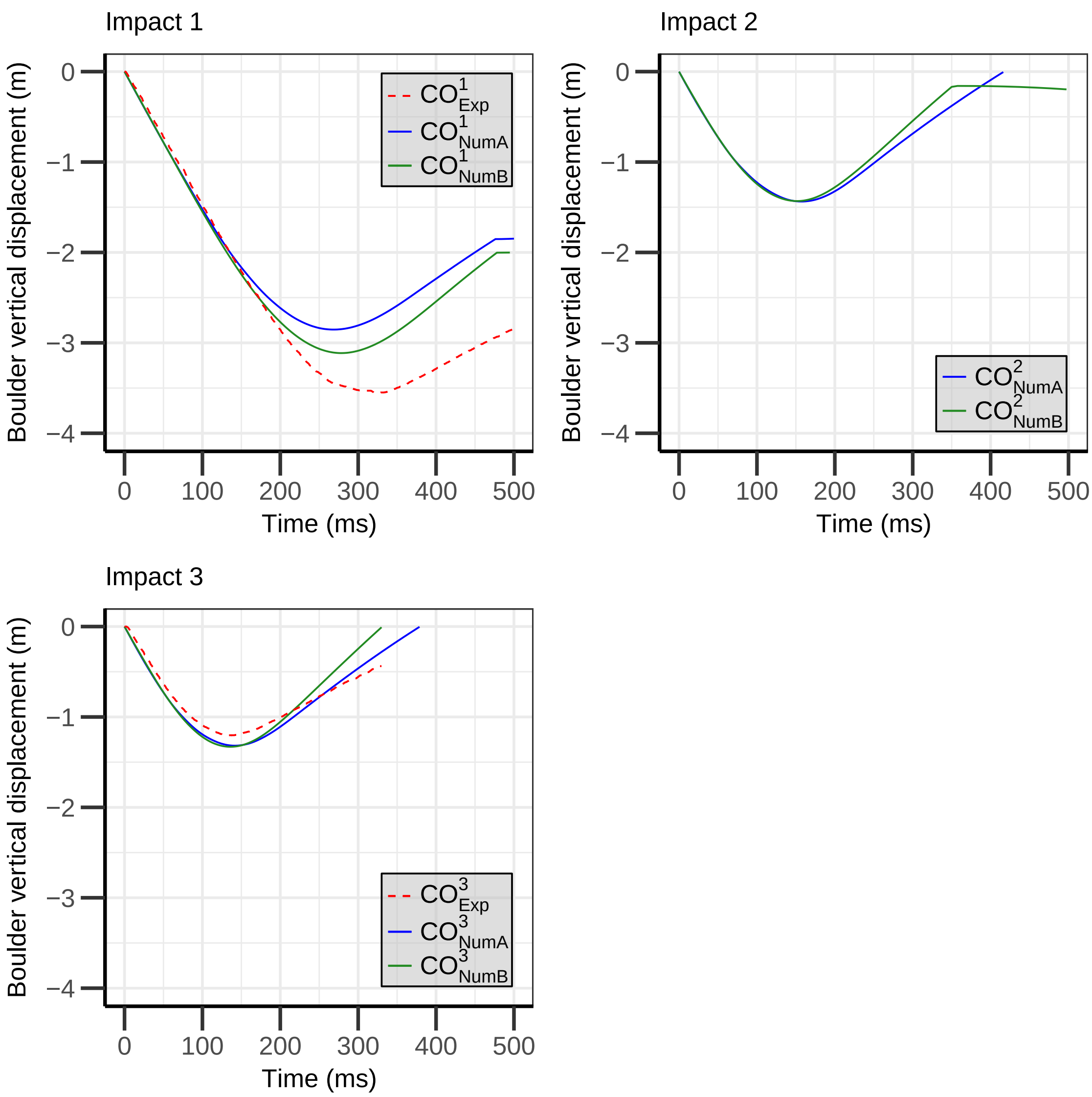

Figure 14: Evolution of the boulder vertical displacement of the net over time for the 3 consecutive impacts: simulation results from models A and B against experimental data.

4. Models predictive capacity

The experimental results (Section 3) show a complex two-phase response of the barrier. They also highlight the influence of the different components on the mechanical response. For example, the net rings subjected to either bending or tensile regimes [Nicot et al., 2001b, Escallón et al., 2014], the energy dissipating devices the response of which depends on the loading conditions [Castanon-Jano et al., 2017] and the connection between the cable and the net [Coulibaly et al., 2019] play major roles in the structure response. In this section, the numerical responses given by

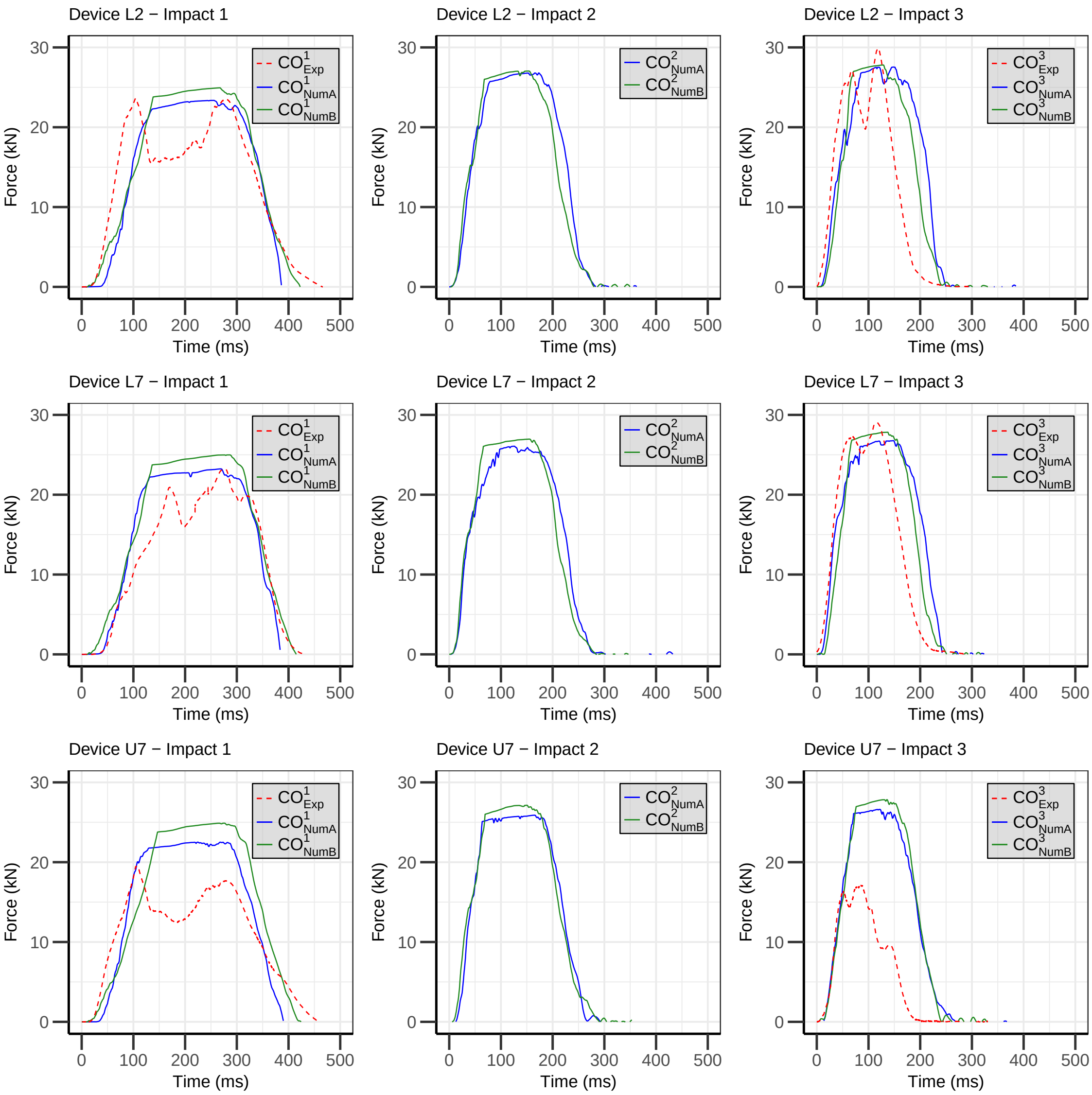

Figure 15: Energy dissipating devices L2, L7 ans U7 force for the 3 consecutive impacts: simulation results from models A and B against experimental data.

	Upper supporting cables				Lower supporting cables			
	A_{UP}	B_{UP}	C_{UP}	D_{UP}	A_{LOW}	B_{LOW}	C_{LOW}	D_{LOW}
Impact 1	17	100	85	0	0	65	60	20
Impact 2	20	185	150	0	0	130	130	20
Impact 3	40	217	205	24	0	182	188	36

Table 5: Experimental cables elongation (sum of the elongations of the two energy dissipating devices connected to the cable) for consecutive impacts. All data are in cm.

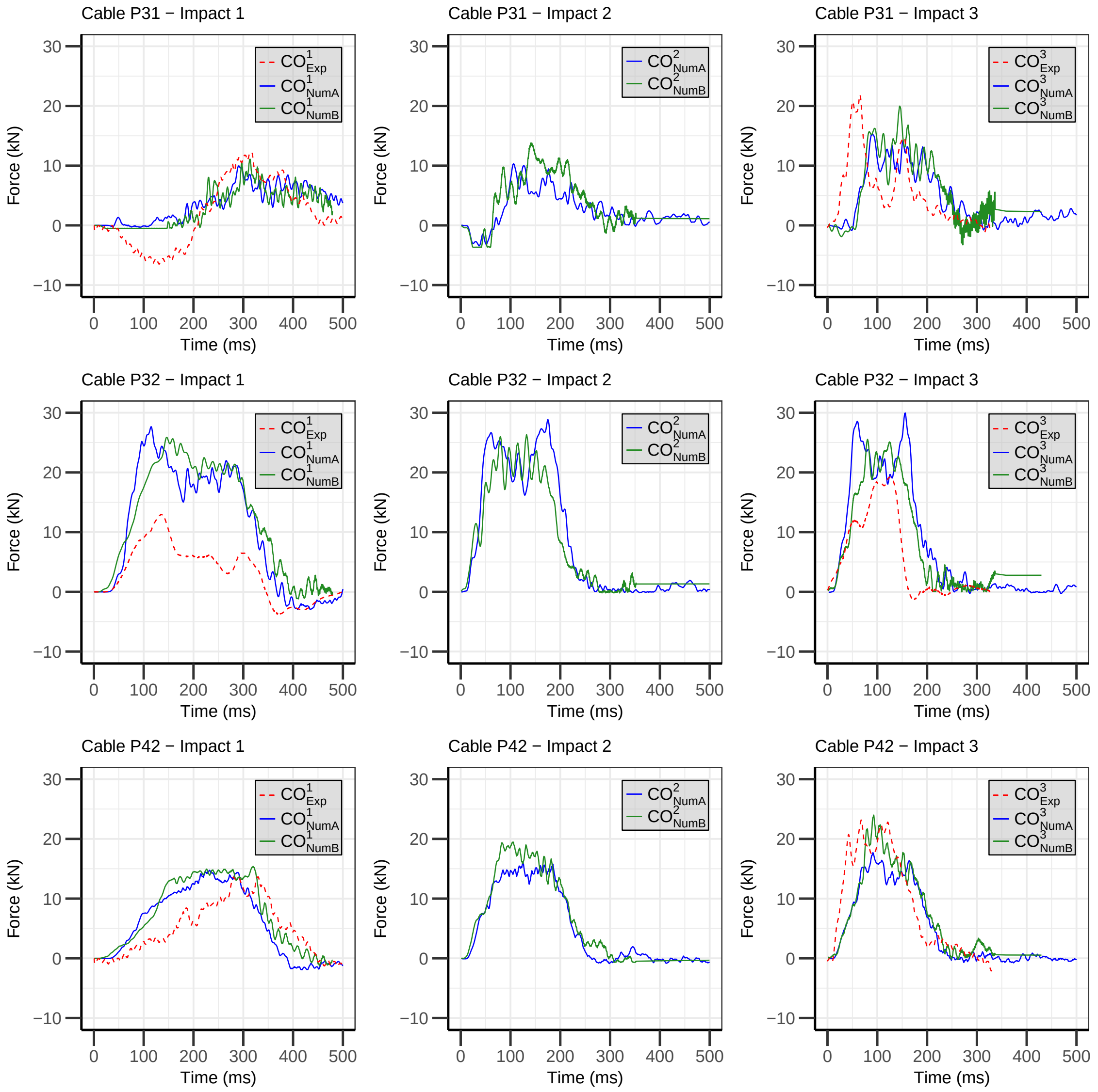

Figure 16: Upstream cables P_{31}, P_{32} and P_{42} force for the 3 consecutive impacts: simulation results from models A and B against experimental data.

the two models for both single and consecutive impacts conditions are analyzed. These predictions are obtained without back analysis on the experimental results. The models predictive capacity is qualitatively and quantitatively explored studying the responses of the global structure, of the energy dissipating devices and of the upstream cables.

4.1. Single impact test

During the single high velocity impact, the structural elements are loaded up to the plasticity limit which needs to be reproduced with the models. Single impact tests were simulated with models A and B, respectively labelled as SI_{NumA} and SI_{NumB}.

The two models qualitatively reproduce the experimental global response of the barrier, the forces into the energy dissipating devices and into the upstream cables. In particular, both models reproduce the pre-tensile and reaction phases observed experimentally (Section 3.1) with the linear and non-linear parts of the boulder vertical displacement curve (Figure 10).

As for the dissipating devices, differences appear between experiments and simulations. In accordance with the dissipating device model implemented, the numerical response shows a sharp increase in the force up to the threshold value, followed by a slightly increasing plateau until the end of the impact. By contrast, experiments reveal significantly different responses in terms of activation force level and post-activation force evolution (Figure 11). The energy dissipating devices experimentally show slightly lower activation values and mean forces during activation. The activation duration is similar (Figure 11) and higher elongations of the energy dissipating devices are observed experimentally (Figure 12). These differences are attributed to the model calibration, based on quasi-static test results. Such a loading has been shown to result in a different response compared to dynamic loading [Castanon-Jano et al., 2017]. Second, the variability in activation force is inherent to the dissipating devices technology. This variability should be considered in the numerical simulations.

Despite the differences in the energy dissipating devices responses, the evolution of the forces for the upstream cables closest (P_{31} and P_{32}) and farthest (P_{42}) from the impact zone are rather well predicted (Figure 13). This demonstrates the models ability in predicting the propagation of the forces inside the structure from the impact zone to the anchors, even at a long distance from the impact zone (cable P_{42}).

In addition to the satisfying qualitative results, the simulations quantitatively compare well to the experimental, with variable accuracy for both models regarding the studied quantities.

The maximum boulder vertical displacement predicted by the simulations (Figure 10) is acceptable when considering the variability of the experimental results (Table 6) (maximum error of 21% : SI_{NumA} vs. SI_{Exp1}). Both models also show acceptable prediction for the maximum forces in the cables (Figure 13).

A lateral symmetry is observed numerically for the force in devices L2 and L7 and for the elongations of cables B and C (Figures 11 and 12) while the experimental evolutions of these quantities exhibit significant asymmetry. Both models also tend to underestimate the lower cables elongation; this is more pronounced for model B (Figure 12). Finally, model A shows slightly higher maximum forces for cables P_{31} and P_{32} and lower ones for cable P_{42} compared to the experiments, while the forces predicted by model B forces are in good agreement with the experiments (Figure 13).

Even though the maximum forces, boulder displacement and elongations of the energy dissipating devices show deviation from the experimental values, the overall trends of the evolution of the forces inside the structure are quite well predicted. This proves that the modeling assumptions made for the main elements of the structure (net, energy dissipating devices, connection between supporting cables and net) are also robust when high intensity loading conditions hold. Considering the global structure, the diffusion of the forces from the impact zone to the anchors is respected. These results validate the global modeling method used for both models in single impact conditions.

	SI_{Exp1}	SI_{Exp2}	SI_{NumA}	SI_{NumB}
Maximum boulder displacement (m)	-4.44	-5.05	-4.00	-4.79

Table 6: Maximum boulder vertical displacement for single impact tests, experimental and numerical results.

4.2. Consecutive impacts test

In consecutive impact conditions, the structure is impacted three times with a lower boulder velocity. The complexity of this loading condition stems from the impact repetition which implies unloading and reloading of the elements of the structure. The two models were tested with con-

	$Displ_{Max}$ (m)			t_{stop} (ms)		
	Exp	model A	model B	Exp	model A	model B
CO^1	3.56	2.85	3.11	325	269	278
CO^2	-	1.44	1.43	166	158	152
CO^3	1.20	1.32	1.33	130	141	136

Table 7: Maximum boulder vertical displacement ($Displ_{Max}$) and time to stop the boulder (t_{stop}), experimental and numerical results for each impact.

secutive impacts: CO^1_{NumA}, CO^2_{NumA} and CO^3_{NumA} for model A, and CO^1_{NumB}, CO^2_{NumB} and CO^3_{NumB} for model B.

The first impact numerical response is qualitatively similar to the single impact one, as observed experimentally in section 3.2. The good prediction of the first impact was expected regarding the good accuracy of the single impact models predictions (Section 4.1). Regarding the subsequent impacts, the stiffening of the structure is predicted by both models with the reduction of the pre-tensile phase duration (Figure 14), the impact duration decreasing (Figure 15) and the maximum forces increasing (Figure 16). The trends for the first and third impacts, as well as the increasing loading rate are predicted for both the energy dissipating devices (Figure 15) and upstream cables evolution of the forces (Figure 16).

Quantitatively, both models show lower maximum boulder displacement for the first impact compared to the experimental results, but a good accuracy is observed for the third impact (Figure 14 and Table 7). The large difference in impact duration between the first and second impact observed numerically confirms that the geometrical reorganization occurs mainly during the first impact. As observed for the single impact test, lower elongation of the energy dissipating devices is obtained due to their modeling assumption and quasi-static calibration (Figure 17). Even though a delay in the loading of the upstream cables is observed, the force in the anchors are predicted from the closest to the farthest of the impact zone (Table 8 and Figure 16).

Overall, the models reproduce the diffusion of the forces into the structure with an accurate timing for each impact. The accuracy increases with the impacts showing that, once the structure geometry after the first impact is predicted, the response of the following impacts is easier to reproduce. However, the prediction of these following impacts implies a good accuracy in the loading and unloading responses of the different structural elements modeling. Moreover, despite differences in the modeling assumptions, the two models show close trends and maximum values in the respective responses.

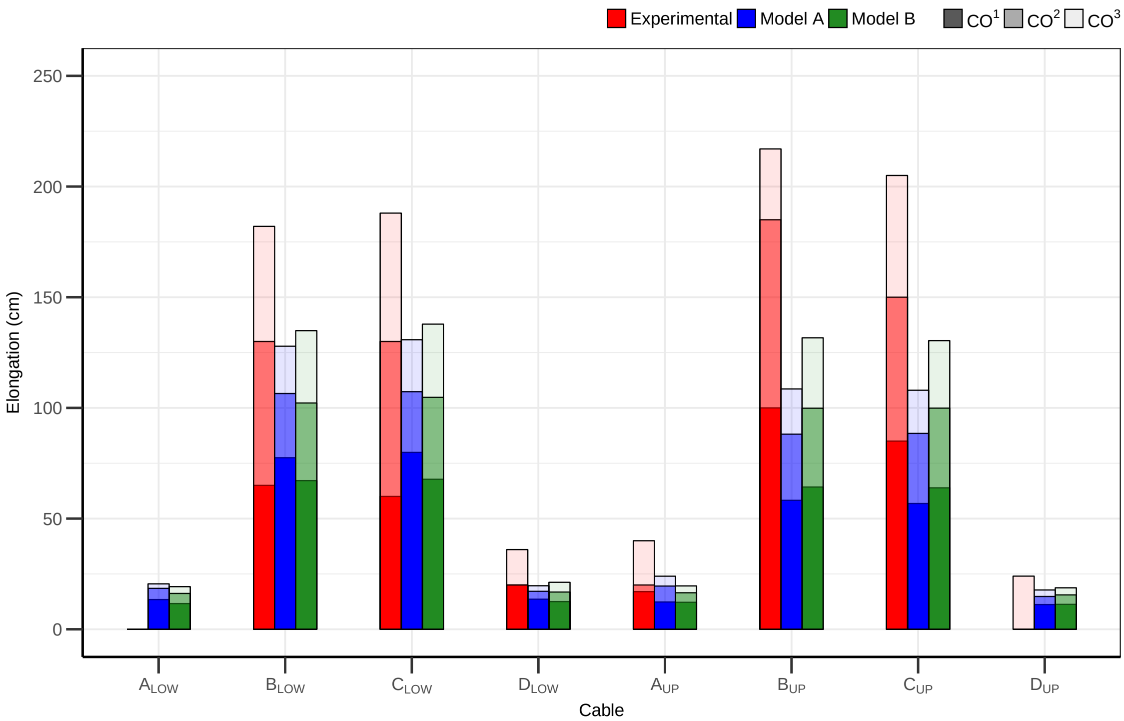

Figure 17: Cables elongation (sum of the elongations of the two energy dissipating devices connected to the cable) for the 3 consecutive impacts: simulation results from models A and B against experimental data.

	Maximum force P_{31} (kN)			Maximum force P_{32} (kN)			Maximum force P_{42} (kN)		
	Exp	model A	model B	Exp	model A	model B	Exp	model A	model B
CO^1	12	10	12	13	28	26	13	16	15
CO^2	-	11	15	-	30	27	-	17	20
CO^3	22	15	20	19	31	26	23	18	25

Table 8: Maximum forces in the upstream cables P_{31}, P_{32}, and P_{42} for each impact: experimental and numerical results.

5. Conclusion

In this paper, the capacities and limitations of DEM modelling approaches for the assessment of the response of rockfall protection barrier were investigated. For that purpose, the response of a 270 kJ in capacity flexible barrier was studied using a subsequent experimental campaign and two discrete element method models.

Experimentally, single impact tests emphasized, despite a significant variability in the structure response, a behavior that consists of a pre-tensile phase followed by a reaction one. For consecutive impacts, the importance of the pre-tensile phase reduces along the impacts, as a consequence of a global stiffening of the structure.

The two models are developed using different codes but the same modeling approach. It consists in modeling and calibrating separately each element of the barrier, and assembling them together to get the full structure model. The models are finally validated in comparison with the experimental full scale tests results without back analysis (single and consecutive impacts). The complexity of both the structure and the impact conditions leads to critical validation conditions for the models, multiple aspects of their responses being explored in details.

The two models exhibit similarities in the modelling of the energy dissipating devices, the posts, the anchors and the boulder. On the contrary, two different approaches with different level of complexity are chosen for modeling the net and cable-net connection, in particular. Despite these differences on these two main structure components, both models allow accurate prediction of the experimental data for single and consecutive impacts, in particular from a qualitative point of view. For single impacts, the pre-tensile and reaction phases are correctly reproduced and the two models are able to predict the large deformations of the structure and the plastic strains occurring. For consecutive impact conditions, the models allow accurate prediction from the first to the third impact which shows that they are able to reproduce fairly the loading and unloading responses of the structure.

Although the comparison between the two models is not the purpose of this study, it is interesting to note that, even if both models reveal ability to predict the response of the structure, some characteristics are sometimes better predicted by one of the two models. For example, model B shows a better accuracy for the boulder vertical displacement (Figure 10) while model A shows a better prediction for the distribution of the energy dissipating devices elongation (Figure 12). This shows that the validation of a numerical model as well as the comparison between different models should not be only limited to one output, but should also consider the structure global response. Indeed, a model can be accurate for some outputs but provide bad predictions for other ones, depending on its initial purpose and level of complexity.

The good predictive capacities of the models show that discrete element method is a well adapted numerical approach for the modeling of flexible rockfall barriers. Indeed, it makes it possible to implement complex behavior laws, including unloading phases, thanks to the explicit Lagrangian formulation of the method. These good predictive capacities also prove the relevance of the calibration procedure based on quasi-static calibration of the different structural elements models, such as the energy dissipating devices or the net.

Finally, considering the acceptable computation time and results, a practical use of these models and of the associated calibration procedures can be considered as a friendly helping tool for the design of new structures, in particular for a preliminary design of new prototypes. However, using these models to get an exact deterministic response of the structure does not seem relevant, because small differences between the real structure and that modeled may have a significant influence on the structure response. For example, the observed asymmetry results from this type of difference and it is not modelled. Finally, these models can be used for more thorough exploration such as parametric analysis, or as training data for meta-models [Toe et al., 2018, Coulibaly et al., 2019].

Acknowledgement

This research was conducted within the frame of the French National project C2ROP. the authors would like to thank all the partners and in particular companies such as CAN and NGE Fondations.

References

A. Albaba, S. Lambert, F. Kneib, B. Chareyre, and F. Nicot. Dem modeling of a flexible barrier impacted by a dry granular flow. *Rock Mechanics and Rock Engineering*, 50(11):3029–3048, Nov 2017. ISSN 1434-453X. doi: 10.1007/s00603-017-1286-z. URL https://doi.org/10.1007/s00603-017-1286-z.

R. D. Andrew, D. A. Fry, and R. E. Bookwalter. *Field Testing and Evaluation of Various Rock Fall Control System*. Chama ValleyProductions, LLC, Chama Valley, NM (USA), 1998.

D. Bertrand, F. Nicot, P. Gotteland, and S. Lambert. Discrete element method (dem) numerical modeling of double-twisted hexagonal mesh. *Canadian Geotechnical Journal*, 45(8):1104–1117, 2008. doi: 10.1139/T08-036. URL https://doi.org/10.1139/T08-036.

D. Bertrand, A. Trad, A. Limam, and C. Silvani. Full-scale dynamic analysis of an innovative rockfall fence under impact using the discrete element method: from the local scale to the structure scale. *Rock Mechanics and Rock Engineering*, 45:885–900, Sept. 2012. doi: 10.1007/s00603-012-0222-5.

F. Bourrier, S. Lambert, and J. Baroth. A reliability-based approach for the design of rockfall protection fences. *Rock Mechanics and Rock Engineering*, 48(1):247–259, Jan 2015. ISSN 1434-453X. doi: 10.1007/s00603-013-0540-2. URL https://doi.org/10.1007/s00603-013-0540-2.

L. Castanon-Jano, E. Blanco-Fernandez, D. Castro-Fresno, and F. Ballester-Muñoz. Energy dissipating devices in falling rock protection barriers. *Rock Mechanics and Rock Engineering*, 50(3): 603 – 619, 2017.

L. Castanon-Jano, E. Blanco-Fernandez, D. Castro-Fresno, and D. Ferreño. Use of explicit fem models for the structural and parametrical analysis of rockfall protection barriers. *Engineering Structures*, 166:212 – 226, 2018. ISSN 0141-0296. doi: https://doi.org/10.1016/j.engstruct.2018.03.064. URL http://www.sciencedirect.com/science/article/pii/S0141029617318461.

A. Cazzani, L. Mongiovì, and T. Frenez. Dynamic finite element analysis of interceptive devices for falling rocks. *International Journal of Rock Mechanics and Mining Sciences*, 39:303–321, 2002.

J. Coulibaly. *Modélisation numérique discrète du comportement mécanique sous impact des structures d'écrans de filets pare-pierres*. PhD thesis, University Grenoble-Alpes, Grenoble (France), 2017a. (in French).

J. Coulibaly, M.-A. Chanut, S. Lambert, and F. Nicot. Toward a generic computational approach for flexible rockfall barrier modeling. *Rock Mechanics and Rock Engineering*, 05 2019. doi: 10.1007/s00603-019-01878-6.

J. B. Coulibaly, M.-A. Chanut, S. Lambert, and F. Nicot. Non-linear discrete mechanical model of steel rings. *Journal of Engineering Mechanics*, 143(9):04017087, 2017b. doi: 10.1061/(ASCE)EM.1943-7889.0001303. URL https://ascelibrary.org/doi/abs/10.1061/%28ASCE%29EM.1943-7889.0001303.

J. B. Coulibaly, M.-A. Chanut, S. Lambert, and F. Nicot. Sliding cable modeling: an attempt at a unified formulation. *International Journal of Solids and Structures*, 130-131:1–10, 01 2018.

EOTA. *Falling Rock Protection Kits. EAD 340059-00-0106, 2018/C 417/07.* European Organization for Technical Approvals, 2018.

J. Escallón, C. Wendeler, E. Chatzi, and P. Bartelt. Parameter identification of rockfall protection barrier components through an inverse formulation. *Engineering Structures*, 77:1 – 16, 2014. ISSN 0141-0296. doi: https://doi.org/10.1016/j.engstruct.2014.07.019. URL http://www.sciencedirect.com/science/article/pii/S0141029614004374.

J. Escallón, v. Boetticher, C. Wendeler, E. Chatzi, and P. Bartelt. Mechanics of chain-link wire nets with loose connections. *Engineering Structures*, 101:68 – 87, 2015. ISSN 0141-0296. doi: https://doi.org/10.1016/j.engstruct.2015.07.005. URL http://www.sciencedirect.com/science/article/pii/S0141029615004393.

K. Feyrer, editor. *Wire Ropes.* Springer, 2015.

W. Gerber and A. Böll. Type-testing of rockfall barriers - comparative results. In *International Symposium Interpraevent*, pages 189–198, Munich (Germany), April 2006.

G. Gottardi and L. Govoni. Full-scale modelling of falling rock protection barriers. *Rock Mechanics and Rock Engineering*, 43(3):261–274, May 2010. ISSN 1434-453X. doi: 10.1007/s00603-009-0046-0. URL https://doi.org/10.1007/s00603-009-0046-0.

J. P. Hambleton, O. Buzzi, A. Giacomini, M. Spadari, and S. W. Sloan. Perforation of flexible rockfall barriers by normal block impact. *Rock Mechanics and Rock Engineering*, 46(3):515–526, 2013.

C. Heiss. Characteristics of the testing of rock fall protection kits on transversal test sites on example "Steirischer Erzberg". In *International Symposium Interpraevent*, pages 49–58, Riva del Garda (Italy), May 2004.

S. Lambert and F. Nicot, editors. *Rockfall Engineering*. Wiley, 2011.

M. T. McCauley, B. W. Works, and S. A. Naramore. *Rockfall Mitigation*. California Department of Transportation, Sacramento, California (USA), 1985.

A. Mentani, A. Giacomini, O. Buzzi, L. Govoni, G. Gottardi, and S. Fityus. Numerical modelling of a low-energy rockfall barrier: New insight into the bullet effect. *Rock Mechanics and Rock Engineering*, 49(4):1247–1262, Apr 2016. ISSN 1434-453X. doi: 10.1007/s00603-015-0803-1. URL https://doi.org/10.1007/s00603-015-0803-1.

A. Mentani, L. Govoni, A. Giacomini, G. Gottardi, and O. Buzzi. An equivalent continuum approach to efficiently model the response of steel wire meshes to rockfall impacts. *Rock Mechanics and Rock Engineering*, Apr 2018. ISSN 1434-453X. doi: 10.1007/s00603-018-1490-5. URL https://doi.org/10.1007/s00603-018-1490-5.

H. Muraishi, M. Samizo, and T. Sugiyama. Development of a flexible low-energy rockfall protection fence. *Quartely Report of Railway Technical Research Institute*, 46(3):161–166, 2005.

F. Nicot, B. Cambou, and G. Mazzoleni. Design of rockfall restraining nets from a discrete element modelling. *Rock Mechanics and Rock Engineering*, 34(2):99–118, 2001a. doi: 10.1007/s006030170017. URL https://doi.org/10.1007/s006030170017.

F. Nicot, B. Cambou, and G. Mazzoleni. From a constitutive modelling of metallic rings to the design of rockfall restraining nets. *International Journal for Numerical and Analytical Methods in Geomechanics*, 25(1):49–70, 2001b.

D. Peila, S. Pelizza, and F. Sassudelli. Evaluation of behaviour of rockfall restraining nets by full scale tests. *Rock Mechanics and Rock Engineering*, 31(1):1–24, Feb 1998. ISSN 1434-453X. doi: 10.1007/s006030050006. URL https://doi.org/10.1007/s006030050006.

D. Smith and J. Duffy. Field test and evaluation of rockfall restraining nets. *California Department of Transportation*, 1990.

M. Spadari, A. Giacomini, O. Buzzi, and J. P. Hambleton. Prediction of the bullet effect for rockfall barriers: a scaling approach. *Rock Mechanics and Rock Engineering*, 45(2):131–144, 2012.

K. Thoeni, C. Lambert, A. Giacomini, and S. W. Sloan. Discrete modelling of hexagonal wire meshes with a stochastically distorted contact model. *Computers and Geotechnics*, 49(Complete): 158–169, 2013. doi: 10.1016/j.compgeo.2012.10.014.

D. Toe, A. Mentani, L. Govoni, F. Bourrier, G. Gottardi, and S. Lambert. Introducing metamodels for a more efficient hazard mitigation strategy with rockfall protection barriers. *Rock Mechanics and Rock Engineering*, 51(4):1097–1109, Apr 2018. ISSN 1434-453X. doi: 10.1007/s00603-017-1394-9. URL https://doi.org/10.1007/s00603-017-1394-9.

P. V. Tran, K. Maegawa, and S. Fukada. Experiments and dynamic finite element analysis of a wire-rope rockfall protective fence. *Rock Mechanics and Rock Engineering*, 46(5):1183–1198, 2013. ISSN 1434-453X. doi: 10.1007/s00603-012-0340-0. URL https://doi.org/10.1007/s00603-012-0340-0.

A. Volkwein. Numerical simulation of flexible rockfall protection systems. In *International Conference on Computing in Civil Engineering*, page 11. ASCE, 2005. doi: 10.1061/40794(179)122. URL https://ascelibrary.org/doi/abs/10.1061/40794%28179%29122.

A. Volkwein, K. Schellenberg, V. Labiouse, F. Agliardi, F. Berger, F. Bourrier, L. K. A. Dorren, W. Gerber, and M. Jaboyedoff. Rockfall characterisation and structural protection – a review. *Natural Hazards and Earth System Sciences*, 11(9):2617–2651, 2011. doi: 10.5194/nhess-11-2617-2011. URL https://www.nat-hazards-earth-syst-sci.net/11/2617/2011/.

V. Šmilauer et al. Using and programming. In *Yade Documentation 2nd ed*. The Yade Project, 2015. doi: 10.5281/zenodo.34043. http://yade-dem.org/doc/.

Z. Yu, Y. Qiao, L. Zhao, H. Xu, S. Zhao, and Y. Liu. A simple analytical method for evaluation of flexible barrier part 1 : Working mechanism and analytical solution. *Advanced Steel Construction*, 14(2):115–141, 04 2018. doi: 10.18057/IJASC.2018.14.2.1.